


Wilson Lee  
Ariana Gonzalez  
Paolo Arguelles  
Ricardo Guevara  
Maria Jose Gonzalez-  
Guerrero  
Frank A. Gomez 

Department of Chemistry and  
Biochemistry, California State  
University, Los Angeles, CA,  
USA

Received February 2, 2018  
Revised March 24, 2018  
Accepted March 26, 2018

## Research Article

# Thread/paper- and paper-based microfluidic devices for glucose assays employing artificial neural networks

This paper describes the fabrication of and data collection from two microfluidic devices: a microfluidic thread/paper based analytical device ( $\mu$ TPAD) and 3D microfluidic paper-based analytical device ( $\mu$ PAD). Flowing solutions of glucose oxidase (GOx), horseradish peroxidase (HRP), and potassium iodide (KI), through each device, on contact with glucose, generated a calibration curve for each platform. The resultant yellow-brown color from the reaction indicates oxidation of iodide to iodine. The devices were dried, scanned, and analyzed yielding a correlation between yellow intensity and glucose concentration. A similar procedure, using an unknown concentration of glucose in artificial urine, is conducted and compared to the calibration curve to obtain the unknown value. Studies to quantify glucose in artificial urine showed good correlation between the theoretical and actual concentrations, as percent differences were  $\leq 13.0\%$ . An ANN was trained on the four-channel CMYK color data from 54  $\mu$ TPAD and 160  $\mu$ PAD analysis sites and Pearson correlation coefficients of  $R = 0.96491$  and  $0.9739$ , respectively, were obtained. The ANN was able to correctly classify 94.4% (51 of 54 samples) and 91.2% (146 of 160 samples) of the  $\mu$ TPAD and  $\mu$ PAD analysis sites, respectively. The development of this technology combined with ANN should further facilitate the use of these platforms for colorimetric analysis of other analytes.

### Keywords:

Artificial neural network / Microfluidic paper-based analytical device / Microfluidics / Microfluidics thread / Paper-based analytical device

DOI 10.1002/elps.201800059



Additional supporting information may be found in the online version of this article at the publisher's web-site

## 1 Introduction

Since its emergence in the early 1990s, the field of microfluidics has continued to expand due to its potential applications in the pharmaceutical, biomedical, and chemical domains among others [1, 2]. The size of the platforms, small sample volume requirements, low cost, fast sampling times, portability, durability, high sensitivity and accuracy, and low power

consumption are a few of the advantages of the technology. For example, current challenges of an aging population, increasing healthcare costs, and the need for modern healthcare methods and delivery to both developed and developing countries, makes microfluidics a leading technology to participate in preventative and personalized medicine in the future [3].

In 2007, Whitesides *et al.* coined the term microfluidic paper-based analytical device ( $\mu$ PAD) and described the first paper-based devices [4–10]. Since then, a myriad of applications typically focused in bioanalysis, healthcare and disease screening have been described [11–20]. A particular strength of  $\mu$ PADs is their use as point-of-care (POC) diagnostic devices for inexpensive colorimetric assays [21, 22] and as paper-based ELISA platforms [23–29]. Paper has been shown to be an excellent platform for microfluidic applications since it is thin, low cost, easy to stack, store and transport, compatible with biological samples, and wicks aqueous liquids without

---

**Correspondence:** Dr. Frank A. Gomez, Department of Chemistry and Biochemistry, California State University, Los Angeles, 5151 State University Drive, Los Angeles, CA 90032–8202, USA  
**Fax:** +323-343-6490  
**E-mail:** fgomez2@calstatela.edu

**Abbreviations:**  $\mu$ PAD, microfluidic paper-based analytical device;  $\mu$ TPAD, microfluidic thread/paper-based analytical device; ANN, artificial neural network; GOx, glucose oxidase; HRP, horseradish peroxidase; POC, point-of-care; GUI, graphical user interface

---

**Color Online:** See the article online to view Figs. 1–4 in color.

the need of active pumping. The combination of the capabilities of paper-based microfluidic systems and lateral flow test strip technology has afforded invaluable options for consumer home healthcare needs. In addition, paper-based devices have a great potential for use in limited-resource settings where a lack of medical infrastructure may exist [30].

The technology involving paper microfluidics have been constantly evolving given its potential as POC diagnostic devices. Advancements in hydrophobic barrier fabrication, device design, and  $\mu$ PAD application have provoked the need for more studies on the optimization and analysis of the paper-based devices [31]. A general trend in  $\mu$ PADs is the use of a single layer of Whatman Grade 1. cellulose chromatography paper as the platform for fabrication, where hydrophobic barriers are patterned onto the paper to form channels that direct fluidic flow. The fabrication of  $\mu$ PADs requires intricate control of channel sizes, allowing efficient and even fluid flow while requiring very small sample sizes. Wax patterning and printing have been shown to be simple to use and highly functional methods to fabricate  $\mu$ PADs [32].

When using wax as a hydrophobic material, there is a need for heating to allow for permeation through the depth of the paper to provide a viable barrier. The heating of wax causes the material to spread laterally across the cellulose paper, thus decreasing optimal channel widths. To overcome this issue, most paper-based devices are designed with only a few channels originating from a central circle. This lowers the amount of possible data points collected using a single  $\mu$ PAD, requiring a separate  $\mu$ PAD to be used for further data collection. A multi-layered  $\mu$ PAD surmounts the need for separate single-layered  $\mu$ PADs, as multiple  $\mu$ PADs can be utilized in a single run. Moreover, enclosed channels protect channels and reagents from external contamination while increasing the wicking rate of fluids.

The recent increase in the use of paper as a viable platform for health-related monitoring has broadened examination of other materials including thread and fabric [33–41]. Thread is an attractive material for microfluidic devices due to its low cost, flexibility, wet-strength, and liquid wicking ability. Furthermore, it is easily manipulated, is available in various structural types, and is usually hydrophilic. We recently detailed a microfluidic thread-based analytical device ( $\mu$ TAD) to determine the activity of the enzyme acetylcholinesterase (AChE) using colorimetric analysis [42]. Similarly, we described a facile ELISA on thread to quantify rabbit IgG [29].

Artificial neural networks (ANNs) are useful methodologies capable of managing nonlinear and complex relations, especially when relationships between experimental data are unknown [43]. Similar to the way a human brain recognizes, manages, and learns patterns in experimental data, ANNs can learn and recognize relations between some independent variables (*i.e.*, input data set) and corresponding dependent variable(s) (*i.e.*, output parameter(s)) [44]. The processing unit in ANNs is an artificial neuron that takes inputs and then generates an output based on associated weights of the inputs. Neurons compute the weighted sum of all of the inputs yielding an output [45]. In recent years, ANNs have been quite

complimentary to response surface methodologies (RSMs) and have successfully been used in various applications including image processing, medicine, environmental science, pharmaceuticals, water resources, and nanotechnology, where statistical methods may not be efficient due to complex relations commonly observed between the data [46–52].

Herein, we describe the fabrication of and data collection from two microfluidic devices, a microfluidic thread/paper based analytical device ( $\mu$ TPAD) and 3D  $\mu$ PAD. By flowing solutions of GOx, HRP, and KI through each device, a calibration curve was generated for each platform. The resultant yellow-brown color from the reaction indicates oxidation of iodide to iodine. The devices were dried, scanned, and analyzed yielding a correlation between yellow intensity and glucose concentrations. For each platform, as a proof of concept, we also demonstrate the effectiveness of ANN fitting and classification algorithms to deduce glucose concentration based on four-channel CMYK color data.

## 2 Materials and methods

### 2.1 Materials

Glucose oxidase (GOx) (174.9 units/mg), horseradish peroxidase (HRP) (179.2 units/mg), potassium iodide, sodium acetate trihydrate, acetic acid, sodium dihydrogen phosphate (mono), disodium phosphate (dibasic), and glucose were purchased from Sigma Aldrich. GOx was prepared in phosphate buffer (0.1 M, pH 6) and HRP was dissolved in acetate buffer (0.2 M, pH 5.1). The GOx/HRP/KI cocktail was prepared by mixing equal volumes of GOx and HRP, and then mixing equal volumes of GOx/HRP solution and 0.6 M KI. Various concentrations of glucose (0.0, 0.5, 1.0, 3.0, 4.5, 6.5, 10, 12.5 and 15.0 mM) were prepared.

Artificial urine solution (pH 6.0) was prepared by mixing ammonium chloride (25 mM), calcium chloride (2.5 mM), citric acid (2.0 mM), magnesium sulfate (2.0 mM), sodium bicarbonate (25 mM), sodium chloride (90 mM), sodium sulfate (10 mM), uric acid (0.4 mM), disodium hydrogen phosphate (7.0 mM), and sodium dihydrogen phosphate (7.0 mM). Varying concentrations of glucose (0.5, 3.0, and 5.0 mM) were added to the artificial urine solution. White #18 100% Nylon thread was purchased from Hobby Lobby. Scotch packaging single sided tape was purchased from a local office supply store. Clear polyester double-sided adhesive tape (AR90445) was purchased from Adhesives Research. For all paper aspects of the platforms, 0.18 mm thick Whatman grade 1 cellulose chromatography paper (GE Healthcare Life Sciences, WA, USA) was used. Wax printing for the 3D- $\mu$ PAD was done using a Colorqube 8580 Solid Ink color printer (Xerox, Norwalk, CT, USA). 3D- $\mu$ PADs were heated on a Hotronix Auto-Open Clam heat press (Stahl's, Sterling Heights, MI, USA). The outer shell apparatus was cut from a sheet of 2.25 mm thick polymethyl methacrylate (PMMA) using a LS-1416 BossLaser CO<sub>2</sub> laser cutter (Boss Laser, Sanford, FL, USA). 0.13 mm thick non-adhesive polymer laminate film

from Zeonex was used as the hydrophobic separating layer for the two sides of the 3D- $\mu$ PADs.

## 2.2 Microfluidic analytical device fabrication

### 2.2.1 $\mu$ TPAD platform fabrication

The platform was fabricated using two pieces of single-sided tape (5.4 cm x 5.4 cm), one piece of double-side tape (5.4 cm x 5.4 cm), three pieces of nylon (2.4 cm), and hole-punched chromatography circles (0.64 cm diameter) (Fig. 1A). A template designed on Inkscape (0.92x, The Inkscape Project, open-source) was used to hole punch the pieces of tape and was designed with a center circle surrounded by nine circles. The bottom layer of the single-sided tape had nine circles hole-punched. Three pieces of nylon thread were trifurcated and layered onto the bottom layer of tape such that the thread would begin at the center circle and each of the trifurcated ends would terminate at the nine holes. The double-sided tape layer had the center and nine circles hole-punched. The bottom side of the double-sided tape had the nine holes covered with pre-spotted paper circles. The chromatography paper circles were pre-spotted with increasing glucose concentrations (5  $\mu$ L) or with artificial urine of known glucose concentration. The topside of the double-sided tape had the center and nine holes covered with blank chromatography paper circles. The top layer single-sided tape was placed on top of the double-sided tape completing the multiplex chip assembly.

To initiate the reaction, GOx/HRP/KI reaction cocktail was spotted (30  $\mu$ L reaction cocktail/45 seconds, 150  $\mu$ L total) onto the center chromatography circle. The reaction cocktail flows through the center chromatography paper circle (inlet), through the nylon thread, up the pre-spotted chromatography paper circles, and terminates at the blank chromatography paper circles where a yellow/brown color is realized, indicating iodine production. After the cocktail (150  $\mu$ L) was flowed into

the chip, it was allowed to sit for 45 s. The chip was air-dried by blowing compressed air over the nine holes on the bottom side of the chip for 5 min and the topside of the chip scanned.

### 2.2.2 3D $\mu$ PAD Fabrication

The 3D- $\mu$ PAD was designed using Inkscape software. In the software, circles and squares were manipulated and oriented to create the multi-channeled  $\mu$ PAD chip. The channel widths (1.0 mm) were determined based on previous studies [32]. The backside of the 3D- $\mu$ PAD cell has eight rectangular channels (1.0  $\times$  3.0 mm), circles midway along the channels (7.0 mm diameter), and a square detection site (5.0  $\times$  5.0 mm) at the end of each channel (Fig. 1B). The 3D- $\mu$ PAD design was duplicated multiple times onto a sheet, printed, and heat pressed (176°C, 120 s). Each sheet was reintroduced to the wax printer and a front layer of protective wax printed onto the surface (Fig. 1B).

The 3D- $\mu$ PAD outer shell apparatus (35  $\times$  35 mm, 6 mm center hole) was cut with a Boss CO<sub>2</sub> laser engraver. One edge was secured together with tape such that a folding apparatus was created. Laminate film was cut to size and was secured to the inside of the shell with tape. Office supply binder clips were used to secure the shell and create even pressure along the edges of the  $\mu$ PAD during the time of reaction.

To initiate the reaction, glucose solutions (5  $\mu$ L) of varying concentrations were pipetted onto the mid-channel circles of the 3D  $\mu$ PAD and let dry for 10 min. Once dried, the  $\mu$ PADs were folded in half with the front side facing inwards and placed into the shell with the laminate sheet separating the two front faces of the 3D- $\mu$ PAD. The hole in the laminate film was filled with two chromatography paper hole-punched circles to bridge the  $\mu$ PAD faces. Upon seating the chip properly into the PMMA shell, the platform was shut and secured along its edge with a binder clip. The GOx/HRP cocktail was spotted (30  $\mu$ L/min for 5 min, 150  $\mu$ L total) through the hole

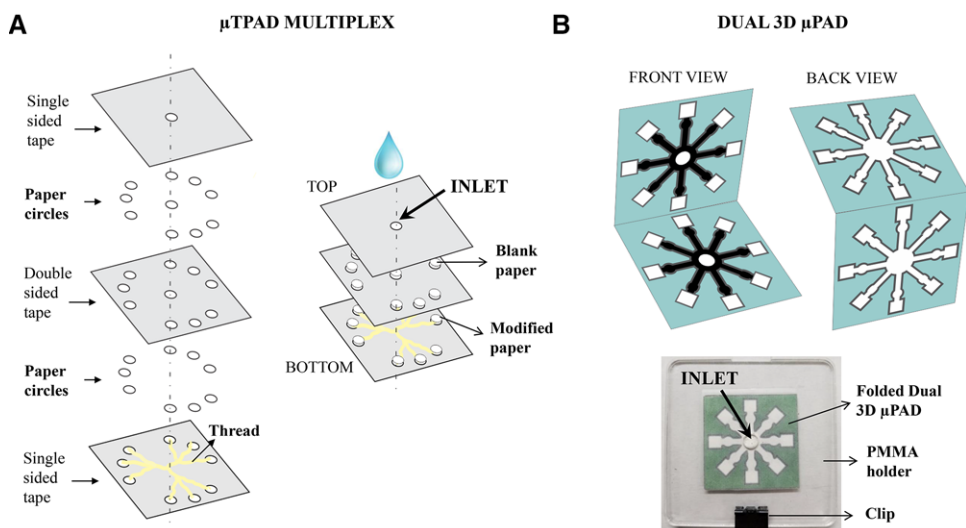


**Figure 1.** (A) Depiction of the different layers and materials defining the  $\mu$ TPAD multiplex. Left side, exploded view of the chip. Right side, chip displaying the blank and the glucose or artificial urine modified paper circles. (B) Top, front (left) and back (right) images of the 3D- $\mu$ PAD Chip. Colors indicate different wax contents; white, green, gray and black displays non, low, medium and complete wax opacity, respectively. Bottom, photograph of the folded 3D- $\mu$ PAD inside the PMMA holder.

in the platform and directly onto the backside of the  $\mu$ PAD. After the final spotting, the  $\mu$ PAD was let dry (10 min). The squares of the chip were filled with the GOx/HRP/KI cocktail and glucose, resulting in a brown-yellow color. The  $\mu$ PADs were removed from the platform and dried evenly with air (5 min) and scanned for colorimetric detection.

### 2.2.3 Microfluidic device analysis

The microfluidic devices were scanned using an Epson Perfection V600 scanner with a resolution of 1600 DPI in preparation for colorimetric analysis. Photoshop CS2 was used to determine the inverse mean, or yellow intensity of each analysis site using the circular marquee tool ( $6.33 \times 6.37$  mm) for the  $\mu$ TPAD, and the square marquee tool ( $5.00 \times 5.00$  mm) for the 3D- $\mu$ PAD. The data were recorded onto an Excel spreadsheet and glucose concentration versus yellow color intensity plotted to create a concentration calibration curve.

### 2.2.4 Artificial neural network design methodology

Mean 16-bit color values from each of the four color channels in the CMYK histogram were extracted into an Excel spreadsheet using Adobe Photoshop. For each chip, the average CMYK color values from the 0 mM control test area were then subtracted from the other test areas each yielding four-component vectors of form  $\Delta \text{CMYK}_i = \langle \Delta C, \Delta M, \Delta Y, \Delta K \rangle$  for each test area, where  $\Delta C = C_i - C_0$  and  $\Delta \text{CMYK}_0 = \langle 0, 0, 0, 0 \rangle$ . The spreadsheet used to train the neural networks consisted of 160 and 54 data points for the  $\mu$ PAD and  $\mu$ TPAD, respectively.

The ANNs were implemented using the Neural Network Toolbox (v9.1) in MATLAB R2016b (v9.1.0.441655). For each of the two proposed chip platforms (*i.e.*  $\mu$ TPAD and  $\mu$ PAD), two analyses were performed: fitting and classification. In all cases, seventy percent of the data points were allotted for a training sample, fifteen percent for a validation sample, and the remaining fifteen percent for an independent testing sample.

For fitting problems, the objective of the neural network is to predict a concentration value given a four-component input vector containing the test area CMYK color data. To achieve this, a two-layer feed-forward neural network with thirty hidden neurons (determined by trial and error to produce the most optimal results) was implemented in MATLAB and trained on an input matrix of size  $4 \times N$  (where  $N = \text{dataset size}$ ; 160 for  $\mu$ PAD, 54 for  $\mu$ TPAD) consisting of CMYK color data, and a target matrix of size  $1 \times N$  consisting of the corresponding known concentration values. The neural network employed a Bayesian regularization backpropagation algorithm to train the network for 1000 epochs. After training, the solution was then deployed as a block into Simulink 7.0. One disadvantage of the fitting algorithm for this application is that it is highly possible for the system to output a value outside the set of known concentrations. For example,

the program may predict the concentration to be 12.38 mM instead of 12.5 mM. To restrict the output, the neural network block was placed in series with a custom MATLAB function block containing a script to discretize the output to the nearest known test strip concentration (see Supporting Information). For instance, raw outputs of 12.38, 11.9, and 13 mM were discretized to 12.5 mM. A custom graphical user interface (GUI) was developed in Simulink to output the raw prediction, its discretized, adjusted value, and the percent error for each.

The performance of the ANN fitting algorithm was quantified using the Pearson correlation coefficient (R), or R-value, which provides a measure of linear dependence between two variables. The correlation coefficient may assume any value between -1 and 1, inclusive. R-values of -1, 0, and 1 indicate perfect negative, independent, and positive correlations, respectively. This metric was used to provide a quantifiable measure of success for the Bayesian backpropagation algorithm used to train the ANN to predict glucose concentration based on color data.

The performance of ANNs applied to fitting problems may be represented by scatter plots (Figs. 2A and 2B). Each data point on the plot indicates a prediction made by the ANN. The location of a data point along the horizontal axis labeled “Target” indicates the “true” glucose concentration of the analysis site, while the location along the vertical axis labeled “Output” indicates the glucose concentration guessed by the ANN. For an ANN with perfect predictive capability, the “Output” values equal the “Target” values, and all data points will reside on the “ $Y = T$ ” identity line, represented by the dotted line on the scatter plot. The Pearson correlation coefficient for a perfect ANN is  $R = 1$ .

For classification problems, the task of a neural network is to sort a sample into a predefined class based on a set of associated inputs. Originally, the aim was for the ANN to classify the data points into one of nine classes (eight classes for  $\mu$ PAD platform), each corresponding to one of the pre-spotted experimental glucose concentrations. However, it was later found that the ANN could not accurately classify test areas at this level of resolution for this particular color change reaction due to high cross-entropy between data points. For this reason, the nine concentration levels were further discretized into three classes roughly corresponding to low, medium, and high glucose concentrations: Class 1 (0, 0.5, 1 mM), Class 2 (3, 4.5, 6.5 mM), and Class 3 (12.5, 10, 15 mM).

To achieve this, a two-layer feed-forward neural network with sixty hidden neurons was implemented in MATLAB and trained on an input matrix of size  $4 \times N$  consisting of CMYK color data, and a binary target matrix of size  $3 \times N$  indicating the corresponding class. The neural network employed a scaled conjugate gradient backpropagation algorithm to train the network for about 20 epochs. The solution was then deployed as a block into Simulink 7.0 and implemented as a custom GUI.

The performance of the ANN classification algorithm was expressed through confusion matrices, square tables with

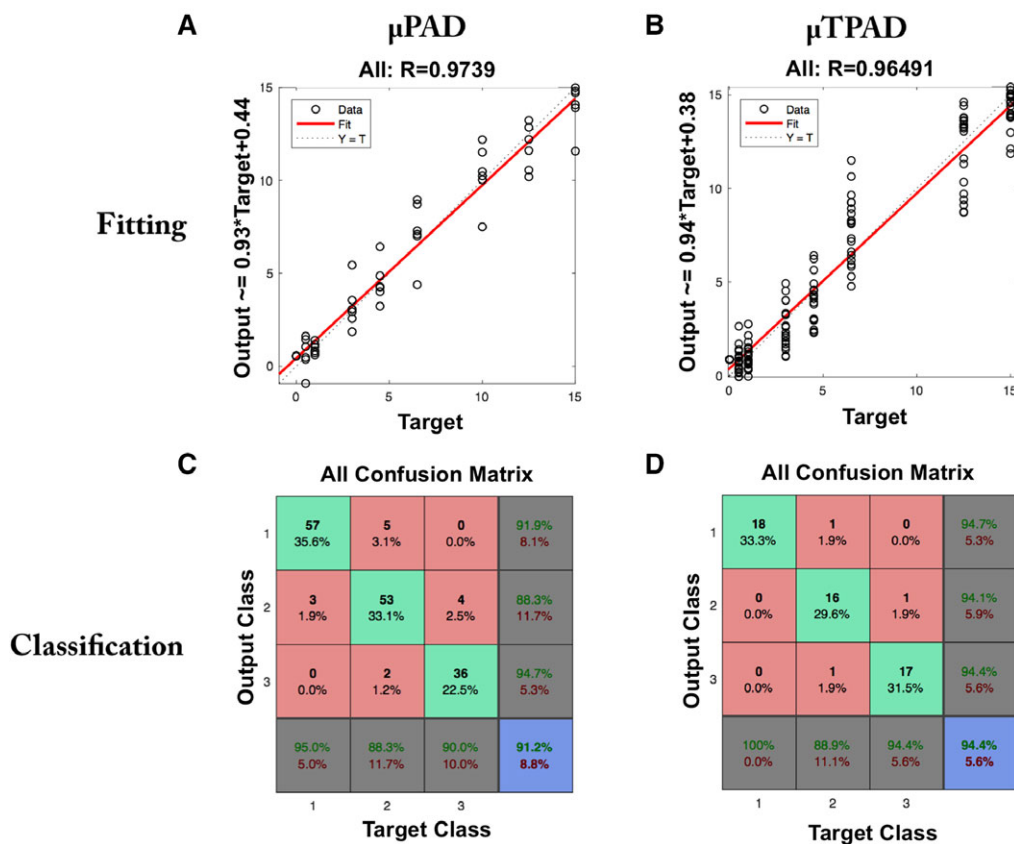


**Figure 2.** At the top, calibration curves from the regression plots created using the neural network fitting program for the (A)  $\mu$ TPAD Multiplex Chip and B) the 3D- $\mu$ PAD. At the bottom, confusion matrix neural network classification program for the C)  $\mu$ TPAD Multiplex Chip and D) the 3D- $\mu$ PAD Chip.

dimensions  $C \times C$  (where  $C$  is the number of possible classes into a dataset may be sorted) that represent the behavior of a classifier. For the  $3 \times 3$  confusion matrices shown in Figs. 2C and 2D, the rows indicate the three “Output” classes into which the ANN may place an analysis site, while the columns indicate the analysis site’s corresponding true, or “Target” class. For instance, the “57” in the cell belonging to the first row and first column of the confusion matrix shown in Fig. 2C indicates that the ANN classifier correctly classified 57 analysis sites belonging to Class 1 as Class 1 sites. The “3” in the cell belonging to the second row and first column of the confusion matrix in the same figure indicates that the ANN classifier misclassified three analysis sites belonging to Class 1 as Class 2 sites. The positive identification rate, or the ratio between number of samples correctly classified and the number of total samples  $N$ , served as a metric to quantify the effectiveness of the classification algorithm.

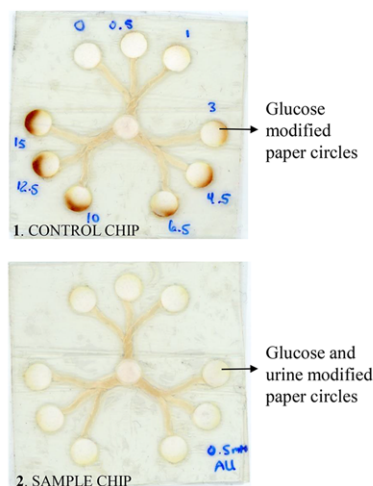
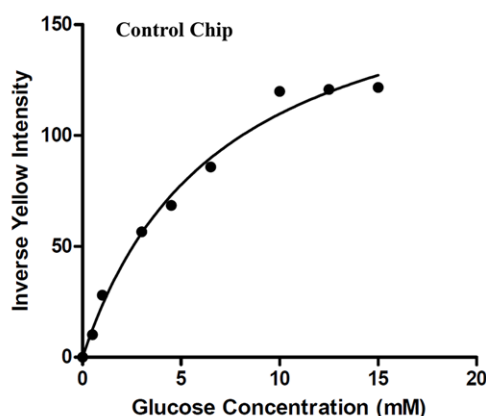
### 3 Results and discussion

To demonstrate the efficacy of the multiplex  $\mu$ TPADs and  $\mu$ PADs systems, glucose was used as an analyte. The glucose assay is based on the enzymatic oxidation of iodide to iodine,

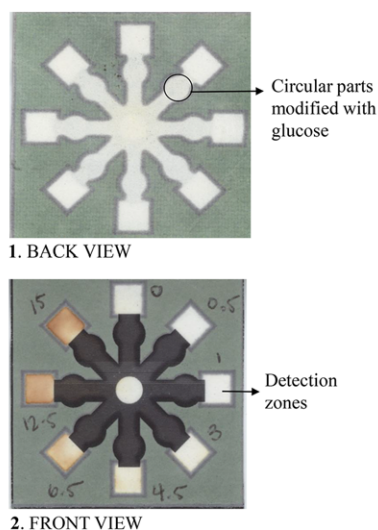
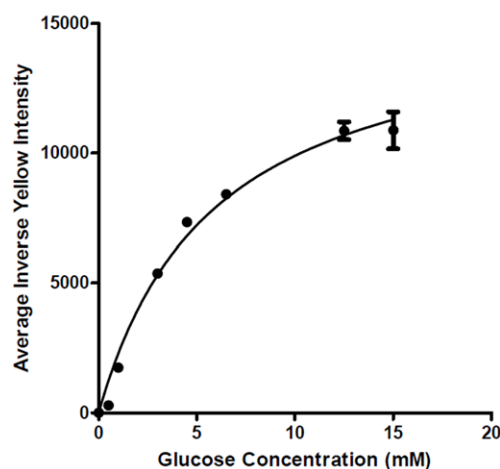
which produces the yellow-brown color (Figs. 3A, 4A). Both microfluidic devices utilized the same analyte system with different magnitudes of color intensity based on each design.

#### 3.1 $\mu$ TPAD detection of glucose

The multiplex  $\mu$ TPADs described in this study were used to demonstrate a reaction can proceed via capillary action in a multilayered device and after completion reaction products can be detected and quantified in the topmost layer of the device. In this study the glucose is oxidized to gluconic acid and oxygen is reduced to hydrogen peroxide by GOx. Hydrogen peroxide is subsequently reduced to water by HRP in association with iodide being oxidized to iodine, which produces the yellow-brown color at the detection sites. The enzymatic reaction occurred in the lower circular piece of chromatography paper. A standard  $\mu$ TPAD chip and a sample chip were run simultaneously to obtain a calibration curve and measure glucose in a sample. Figure 3A shows the scans of the standard chip with increasing glucose concentrations and of the 0.5 mM glucose sample chip. As seen from the standard  $\mu$ TPAD, as the concentration of glucose increases, the yellow-brown color also intensifies. For the sample chip, the yellow intensity observed is about the same throughout

**A**  $\mu$ TPAD MULTIPLEX**B** CALIBRATION CURVE  $\mu$ TPAD MULTIPLEX

**Figure 3.** (A) Pictures of the  $\mu$ TPAD multiplex. In 1, Control chip in which differences in color intensities was used for analyzing subsequent sample chips. Numbers (in blue) indicate different concentrations of glucose immobilized in the paper circles. In 2, example of a sample chip with paper circles modified using a fixed concentration of artificial urine and 0.5 mM glucose. (B) Calibration curve obtained from the control  $\mu$ TPAD chip of the inverse yellow intensity as a function of the glucose concentration. The calibration curve was used to measure unknown glucose contents in urine samples.

**A** DUAL 3D  $\mu$ PAD**B** CALIBRATION CURVE DUAL 3D  $\mu$ PAD

**Figure 4.** (A) Pictures of the 3D- $\mu$ PAD Chip. Top, back view of the chip pre-spotted with different concentrations of glucose. Bottom, front side of the same chip. Increasing color intensities inside the squares indicate the increasing glucose concentrations used in the pre-spotted areas. (B) Calibration curve obtained using the front side of the 3D- $\mu$ PAD of the inverse yellow intensity as a function of the glucose concentration.

since the glucose concentration is identical, indicating that the GOx/HRP/KI cocktail spread equally into the nylon channels. Figure 3B shows one of the saturation curves produced of the corrected inverse yellow intensities as a function of glucose concentration. The increase in yellow intensity produced correlates with the increasing glucose concentration. The calibration curves obtained were used to measure the glucose concentration of the sample chip that was run simultaneously.

The sample  $\mu$ TPAD was run to examine the ability of multiplex  $\mu$ TPADs to measure glucose in artificial urine. Three artificial urine solutions with glucose concentrations of 0.5, 3.0, and 5.0 mM were used. The sample  $\mu$ TPAD provided a total of nine detection sites and the yellow intensities of the nine analysis sites were averaged. Using the Michaelis-Menten equation produced by the calibration curve obtained from analyzing the standard chip using Photoshop,

**Table 1.** Comparison of known glucose concentrations to glucose concentrations detected by analysis, with percent difference

Known glucose concentration (mM)	Detected concentration (mM)	Percent difference
0.5	0.57 ± 0.05	13.08
3.0	2.67 ± 0.23	11.64
5.0	4.87 ± 0.09	2.63

the glucose concentration of the sample chip was determined. The observed glucose concentrations and corresponding standard deviations are stated in Table 1. The percent differences calculated between the actual glucose concentration and the concentration obtained using the calibration curve indicate the error associated with the detected concentrations.

As seen from Table 1, all the percent differences were less than or equal to 13.0%, indicating that the calibration curves produced by the standard chips were able to measure the glucose concentration of the sample chip precisely. The values provided in the table were obtained from running a single sample and standard chip simultaneously. The normal glucose concentration in urine ranges from 0.0 to 0.8 mM. Hence, the results demonstrate that the multiplex  $\mu$ TPADs yield accurate, quantitative results within the range of both a healthy and possibly diabetic patient. The LOD for the device was 0.5 mM.

An ANN was trained on the four-channel CMYK color data from 54  $\mu$ TPAD analysis sites to evaluate the ability of fitting and classification machine learning algorithms to deduce glucose concentration for a thread- and paper-based microfluidic platform. Figure 2B shows the Pearson correlation coefficient to be  $R = 0.96491$ , indicating a highly linearly dependent relationship between the two variables, and excellent ANN fitting performance. The confusion matrix shown in Fig. 2D indicates that the ANN correctly classified 94.4% (51 of 54 samples) of  $\mu$ TPAD analysis sites, indicating excellent ANN classification performance. The ANN was able to correctly identify all Class 1 analysis sites, and made no errors distinguishing between Class 1 and Class 3 sites. Three errors, each with one instance of occurrence (each accounting for 1.9% of the total number of classifications), were made: misclassifying a Class 2 site as a Class 1 site, a Class 3 site as a Class 2 site, and a Class 2 site as a Class 3 site.

### 3.2 3D- $\mu$ PAD detection of glucose

The 3D- $\mu$ PAD designed for this study was created with the goal of increasing the amount of data collected in a short period of time. As previously explained, the oxidation of glucose to gluconic acid and reduction of  $O_2$  to  $H_2O_2$  by GOx, and oxidation of iodide to iodine by HRP produces the yellow-brown color observed at the analysis area pictured in Fig. 4A. The enzymatic reaction occurred as the solutions travelled through the chromatography paper channels into the square detection sites. Due to the limitations of the x-y plane of a piece of cellulose chromatography paper, the z-plane had to be utilized in a way that would contribute to the overall compact yet versatile  $\mu$ PAD platform. In this case, a two-sided 3D- $\mu$ PAD allows a reaction to go to completion via transfer of solution via capillary action between the two faces of the device.

A standard  $\mu$ PAD chip allows for rapid detection of analyte on a lateral plane, but given the thinness of a single sheet of paper, multiple layers of a given  $\mu$ PAD design could be run simultaneously. Figure 4A shows a scan of the chip with increasing glucose concentrations. Mentioned previously, as glucose concentration increases, the observed yellow-brown color also intensifies, evidenced by Fig. 4B. One advantage to the 3D- $\mu$ PAD is the optimization of the design wherein the square analysis sites provide a homogenous mixture site. That is, the GOx/HRP/KI cocktail spreads evenly into the

squares and the transfer of solution between the bottom and top face of the  $\mu$ PAD was complete, again evidenced by the low relative standard deviations of values. Figure 4B shows one of the curves produced by the inverse yellow intensities as a function of glucose concentration.

The 3D- $\mu$ PAD design can theoretically be used to run 16 different concentrations of analyte, or multiple differing concentrations of an unknown concentration. In this study, varying concentrations (0.5, 1, 3, 4.5, 6.5, 12.5, and 15 mM) were used. The yellow intensities of the eight analysis sites were averaged and a curve produced. As with the  $\mu$ TPAD, the LOD for the 3D- $\mu$ PAD device was 0.5 mM.

An ANN was trained on the four-channel CMYK color data from 160  $\mu$ PAD analysis sites to evaluate the ability of fitting and classification machine learning algorithms to deduce glucose concentration for a 3D paper-based microfluidic platform. Figure 2A shows the Pearson correlation coefficient was  $R = 0.9739$ , indicating a highly linearly dependent relationship between the two variables, and excellent ANN performance. The confusion matrix shown in Fig. 2C indicates that the ANN has correctly sorted 91.2% (146 of 160 samples) of the  $\mu$ PAD analysis sites. The errors the ANN was most likely to make were misclassifying a Class 2 site as a Class 1 site, which occurred in 3.1% (5 of 160 samples) of the data points, and misclassifying a Class 3 site as a Class 2 site, which occurred 2.5% (4 of 160 samples) of the data points. The ANN made no errors distinguishing between Class 1 and Class 3 sites.

## 4 Concluding remarks

We have described the design and fabrication of two microfluidic devices that were fabricated and optimized for a glucose assay with detection of glucose concentrations ranging from 0.5 to 15 mM. The integration of the data collected from the microfluidic devices into an ANN system utilized a deep learning algorithm for colorimetric detection of analytes to enzymatically detect glucose. A  $\mu$ TPAD and 3D- $\mu$ PAD devices were fabricated and a calibration curve was generated for both systems by flowing solutions of GOx, HRP, and KI onto the device centers. The capillary action and lateral flow reached the glucose spots of increasing concentrations and a clear to yellow-brown color change observed at the analysis spot for each device. In the  $\mu$ TPAD chip, an unknown concentration of glucose in artificial urine was tested and compared to the calibration curve to obtain the unknown concentration value.

We have also demonstrated the ability of a machine-learning approach to computationally interpret the results of thread/paper- and paper-based analytical devices.

Lapses in the ability of the ANN to form a representative and well-generalized relationship between four-channel CMYK data as system inputs and glucose concentration as system outputs may be attributable to the relative lack of color variability in the observed color changes. This invariance results in high cross-entropy, limiting the pattern recognition

capability of the ANN. However, a higher predictive resolution may be attained by chemically amplifying the color changes and training the ANN on a larger data set. Of the two platforms analyzed, the 3D- $\mu$ PAD is more practical for integration with ANN-based analytics due to its high degree of reproducibility and speed of production, allowing for large training datasets to be built in short periods of time.

For point-of-care diagnostic applications, users will likely not have access to a scanner or spectrophotometric instrument to extract digital color values from the completed assay and perform colorimetric analysis. ANNs may also be used to standardize differing lighting conditions across multiple assays by referencing a color calibration area on the assay itself. This may be a white, true black, or 18% gray middle reference card. A program that can normalize color values may be implemented using the MATLAB Image Processing Toolbox, among numerous well-documented methods. The effectiveness of an ANN-based lighting normalization algorithm will only increase as the system is trained on more data points.

In many ways, the fields of microfluidics and machine learning are complementary; inexpensive and highly reproducible analytical devices can provide the large datasets needed for ANNs to function well. The relative low cost and ease-of-reproducibility of the microfluidic devices described here combined with the high scalability of ANN-based algorithms through smartphone applications and other software deployment solutions make such a system ideal for rapid, POC diagnostics.

*The authors gratefully acknowledge financial support for this research by grants from the National Science Foundation (HRD-1547723, EEC-0812348, IIA-1448166), and the W. M. Keck Foundation.*

*The authors have no relevant affiliations or financial involvement with an organization or entity with a financial interest in or financial conflict with the subject matter or materials discussed in the manuscript. This includes employment, consultancies, honoraria, stock ownership or options, expert testimony, grants or patents received or pending, or royalties. No writing assistance was utilized in the production of this manuscript.*

## 5 References

- [1] Manz, Z., Graber, N., Widmer, H. M., *Sensor Actuat. B Chem.* 1990, 1, 244–248.
- [2] Avoundjian, A., Jalali-Heravi, M., Gomez, F. A., *Anal. Bioanal. Chem.* 2017, 409, 2697–2703.
- [3] Gomez, F. A., *Bioanalysis* 2014, 6, 2911–2914.
- [4] Martinez, A. W., Phillips, S. T., Butte, M. J., Whitesides, G. M., *Angew. Chem., Int. Ed.* 2007, 46, 1318–1320.
- [5] Martinez, A. W., Phillips, S. T., Carrilho, E., Thomas III, S. W., Sindi, H., Whitesides, G. M., *Anal. Chem.* 2008, 80, 3699–3707.
- [6] Bruzewicz, D. A., Reches, M., Whitesides, G. M., *Anal. Chem.* 2008, 80, 3387–3392.
- [7] Martinez, A. W., Phillips, S. T., Wiley, B. J., Gupta, M., Whitesides, G. M., *Lab Chip* 2008, 8, 2146–2150.
- [8] Martinez, A. W., Phillips, S. T., Whitesides, G. M., Carrilho, E., *Anal. Chem.* 2010, 82, 3–10.
- [9] Schilling, K. M., Lepore, A. L., Kurian, J. A., Martinez, A. W., *Anal. Chem.* 2012, 84, 1579–1585.
- [10] Cheng, C. M., Mazzeo, A. D., Gong, J. L., Martinez, A. W., Phillips, S. T., Jain, N., Whitesides, G. M., *Lab Chip* 2010, 10, 3201–3205.
- [11] Rodriguez, N. M., Wong, W. S., Liu, L., Dewar, R., Klapperich, C. M., *Lab Chip*, 2016, 16, 753–763.
- [12] Kim, W. S., Shin, J. H., Park, H. K., Choi, S., *Sensor Actuat. B Chem.* 2016, 222, 1112–1118.
- [13] Ueland, M., Blanes, L., Taudte, R. V., Stuart, B. H., Cole, N., Willis, P., Roux, C., Doble, P., *J. Chromatogr. A*, 2016, 1436, 28–33.
- [14] Jang, I., Song, S., *Lab Chip* 2015, 15, 3405–3412.
- [15] Zhang, Y., Zuo, P., Ye, B. C., *Biosens. Bioelectron.* 2015, 68, 14–19.
- [16] Jin, S. Q., Guo, S. M., Zuo, P., Ye, B. C., *Biosens. Bioelectron.* 2015, 63, 379–383.
- [17] Yang X., Reavis, H. D., Roberts, C. L., Kim, J. S., *Anal. Chem.* 2016, 88, 7904–7909.
- [18] Park, T. S., Li, W., McCracken, K. E., Yoon, J.-Y., *Lab Chip* 2013, 13, 4832–4840.
- [19] Ferrer, I. M., Valadez, H., Estala L., Gomez F. A., *Electrophoresis* 2014, 35, 2417–2419.
- [20] Renault, C., Koehne, J., Ricco, A. J., Crooks, R. M., *Langmuir* 2014, 30, 7030–7036.
- [21] Lee, D. S., Jeon, B. G., Ihm, C., Park, J. K., Jung, M. Y., *Lab Chip* 2011, 11, 120–126.
- [22] Nash, M. A., Hoffman, J. M., Stevens, D. Y., Hoffman, A. S., Stayton, P. S., Yager, P., *Lab Chip* 2010, 10, 2279–2282.
- [23] Wang, S., Ge, L., Song, X., Yu, J., Ge, S., Huang, J., Zeng, F., *Biosens. Bioelectron.* 2012, 31, 212–218.
- [24] Martinez, A. W., *Bioanalysis* 2011, 3, 2589–2592.
- [25] Cheng, C. M., Martinez, A. W., Gong, J., Mace, C. R., Phillips, S. T., Carrilho, E., Mirica, K. A., Whitesides, G. M., *Angew. Chem., Int. Ed.* 2010, 49, 4771–4774.
- [26] Hsu, C.-K., Huang, H.-Y., Chen, W.-R., Nishie, W., Ujiiie, H., Natsuga, K., Fan, S.-T., Wang, H.-K., Lee, J. Y.-Y., Tsai, W.-L., Shimizu, H., Cheng, C.-M., *Anal. Chem.* 2014, 86, 4605–4610.
- [27] Murdock, R. C., Shen, L., Griffin, D. K., Keely-Loughnane, n., Papautsky, I., Hage, J. A., *Anal. Chem.* 2013, 85, 11634–11642.
- [28] Hsu, M.-Y., Yang, C.-Y., Hsu, W.-S., Lin, K.-H., Wang, C.-Y., Shen, Y.-C., Chen, Y.-C., Chau, S.-F., Tsai, H.-Y., Cheng, C.-M., *Biomaterials* 2014, 3729–3735.
- [29] Gonzalez, A., Gaines, M., Gallegos, L. Y., Guevara, R., Gomez, F. A., *Electrophoresis* 2018, 39, 476–484.
- [30] Syedmoradi, L., Gomez, F. A., *Bioanalysis*, 2017, 9, 841–843.
- [31] Jeong, S. G., Lee, S. H., Choi, C. H., Kim, J., Lee, C. S., *Lab Chip* 2015, 15, 1188–1194.
- [32] Lee, W., Gomez, F. A., *Micromachines*, 2017, 8, 99.



- [33] Li, X., Tian, J., Shen, W., *ACS Appl. Mater. Interfaces* 2010, 2, 1–6.
- [34] Safavieh, R., Zhou, G. Z., Juncker, D., *Lab Chip* 2011, 11, 2618–2624.
- [35] Reches, M., Mirica, K. A., Dasgupta, R., Dickey, M. D., Butte, M. J., Whitesides, G. M., *ACS App. Mater. Interfaces* 2010, 2, 1722–1728.
- [36] Bhandari, P., Narahari, T., Dendukuri, D., *Lab Chip* 2011, 11, 2493–2499.
- [37] Nilghaz, A., Wicaksono, D. H. B., Gustiono, D., Abdul Majid, F. A., Supriyanto, E., Abdul Kadir, M. R., *Lab Chip* 2012, 12, 209–218.
- [38] Nilghas, A., Ballerini, D. R., Shen, W., *Biomicrofluidics* 2013, 7, 051501-1-15.
- [39] Mostafalu, P., Akbari, M., Alberti, K. A., Khademhosseini, A., Sonkusale, S. R., *Microsystems Nanoengineering* 2016, 2, 16039-1-16039-10.
- [40] Glavan, A. C., Ainla, A., Hamed, M. M., Fernandez-Abdeul, M. T., Whitesides, G. M., *Lab Chip* 2016, 16, 112–119.
- [41] Zhou, G., Mao, X., Juncker, D., *Anal. Chem.* 2012, 84, 7736–7743.
- [42] Liu, C., Gomez, F. A., *Electrophoresis* 2017, 38, 1002–1006.
- [43] Agatonovic-Kustrin, S., Beresford, R., *J. Pharm. Biomed. Anal.* 2000, 22, 717–727.
- [44] Egmont-Petersen, M., de Ridder, D., Handels, H., *Pattern Recognit.* 2002, 35, 2279–2301.
- [45] Ali, H. S. M., Blagden, N., York, P., Amani, A., Brook, T., *Eur. J. Pharm. Sci.* 2009, 37, 514–522.
- [46] Peh, K. K., Lim, C. P., Quek, S. S., Khoh, K. H., *Pharm Res.* 2000, 17, 1384–1389.
- [47] Amani, A., Mohammadyani, D. Artificial neural networks: applications in nanotechnology. In: Hui, C-L, *Artificial neural networks—application*. Rijeka: INTECH, 2011.
- [48] Aghajani, M., Shahverdi, A. R., Amani, A., *AAPS Pharm-SciTech* 2012, 13, 1293–1301.
- [49] Esmaeilzadeh-Gharedaghi, E., Faramarzi, M. A., Amini, M. A., Najafabadi, A. R., Rezayat, S. M., Amani, A., *Pharm. Dev. Tech.* 2012, 17, 638–647.
- [50] Orimoto, Y., Watanabe, K., Yamashita, K., Uehara, M., Nakamura, H., Furuya, T., Maeda, H. J., *Phys. Chem. C* 2012, 116, 17885–17896.
- [51] Fakhrabadi, M. M. S., Samadzadeh, M., Rastgoo, A., Yazdi, M. H., Mashhadi, M. M., *Physica E: Low Dimens. Syst. Nanostruct.* 2011, 44, 565–578.
- [52] Ahadian, S., Mizuseki, H., Kawazoe, Y., *Microfluid. Nanofluidics* 2010, 9, 319–328.